Accepted Manuscript

Low-temperature synthesis of two-dimensional nanostructured Co_3O_4 and improved electrochemical properties for lithium-ion batteries

Zhongpei Lu, JingJing Ding, Xuehong Lin, Yang Liu, Haitao Ye, Gang Yang, Fan Yin, Bo Yan

PII: S0032-5910(16)30964-0
DOI: doi:10.1016/j.powtec.2016.12.081
Reference: PTEC 12229

To appear in: *Powder Technology*

Received date: 3 October 2016
Revised date: 17 December 2016
Accepted date: 27 December 2016

Please cite this article as: Zhongpei Lu, JingJing Ding, Xuehong Lin, Yang Liu, Haitao Ye, Gang Yang, Fan Yin, Bo Yan, Low-temperature synthesis of two-dimensional nanostructured Co_3O_4 and improved electrochemical properties for lithium-ion batteries, *Powder Technology* (2016), doi:10.1016/j.powtec.2016.12.081

Low-Temperature Synthesis of Two-Dimensional Nanostructured Co_3O_4 and Improved Electrochemical Properties for Lithium-Ion Batteries

Zhongpei Lu,[a,b] JingJing Ding,[b] Xuehong Lin,[b] Yang Liu,[b] Haitao Ye,[c] Gang Yang,[*a,b] Fan Yin,[*a,b] Bo Yan[c]

[a.] School of Biology and Chemical Engineering, Jiangsu University of Science and Technology, Zhenjiang 212003, PR China

[b.] Department of Chemistry and Materials Engineering, Changshu Institute of Technology, Changshu 215500, P. R. China

[c.] School of Engineering and Applied Science, Aston University, Birmingham B4 7ET, United Kingdom

* To whom correspondence should be addressed:

Tel: 86-512-52251843, Fax: 86-512-52251842

E-mail: gyang@cslg.edu.cn

Abstract

Urea as a cheap reagent is very useful in preparation two-dimensional metal oxides with tunable crystal morphologies, while refluxing method is a simple route to control the decomposition of urea. Here, a low temperature refluxing in the presence of urea is developed to prepare porous Co_3O_4 as anode material for lithium-ion batteries. The self-assembly cobalt hydrotalcite-like compounds (Co-HLC) is firstly synthesized through refluxing the mixture of cobaltous nitrate and urea. After pyrolysis, the flower-like morphology of Co-HLC is successfully maintained in the final product of Co_3O_4. The ordered two-dimensional Co_3O_4 nanosheets provide good contact with electrolyte and stable porous structure during lithiation/delithiation. Co_3O_4-120 synthesized under refluxing temperature of 120 °C shows the initial charge capacities of 722 and 741 mAh g^{-1} at the 2nd and 100th cycle under 100 mA g^{-1}. Moreover, Co_3O_4-120 as electrode for a supercapacitor presents excellent capacitance, 167 F g^{-1} after 3000 cycles at 1 A g^{-1}. Under 5, 10 and 20 A g^{-1}, Co_3O_4-120 electrode delivers 128, 104 and 90 F g^{-1}, respectively. The porous structure in Co_3O_4 with enhanced electrochemical performance indicates low temperature refluxing preparation is an applicable and energy-saved method to synthesize transitional metal oxide with tunable crystal morphologies.

Key words: lithium-ion batteries; anode materials; hydrotalcite-like compounds; metal oxide; refluxing; electrochemical performance.

1. Introduction

Lithium-ion batteries (LIBs), a dominant power source for portable electronic devices, have received growing attention under the increasing environmental demand [1,2]. Until now, graphite is the most widely used commercial anode for LIBs because it offers both electrochemical and mechanical stability. However, graphite provides low theoretical capacity of 372 mAh g^{-1} and poor rate performance [3,4]. Seeking alternative anode materials has become an urgent task. In recent years, there is growing interest in metallic anode for LIBs, such as Si [5,6], Sn [7-9], and Sb [10], etc. Though metallic anodes are cheap and safe, the fatal conflict between the large volume change and capacity hinders the metallic anodes to replace the graphite for LIBs [11,12].

As the primary method for suppressing volume change of anode, metal oxides with the buffer against volume expansion become potential anode materials for high-performance LIBs [13-15]. Reddy et al. comprehensively reviewed the electrochemical Li storage and cycling properties of binary, ternary, and complex metal oxides and oxalates in which their work described the efforts to develop alternative anode materials for high-performance LIBs in detail [15].

Transition metal oxides [16-23], such as Co_3O_4, SnO_2, FeO_x, MnO_x, CuO and NiO et al. have been widely studied as potential anode materials for LIBs due to the high specific capacities, high rate performance and stability. Co_3O_4 has attracted the attention because of its stable crystal structure and high theoretical capacity (890 mAh g^{-1}) [23-27]. Cobaltous hydroxide, carbonate, oxycarbonate, oxalate, acetate, or sulfate, can facilely convert to Co_3O_4 upon 300 °C in air, and the morphology of the initial salt can be retained. It is accepted that the electrochemical performance of Co_3O_4 depends on the particle sizes, shapes and morphological structures [25-29]

Co_3O_4 has been synthesized by various routes [29-33], such as co-precipitation, molten salt synthesis, solvothermal, microwave-hydrothemal and ultrasonic method etc. For example, Wang et al. reported Co_3O_4 hierarchical microstructures which was converted from hexagonal porous nano-plates by hydrothermal [34]. Beside co-precipitation [35], hydrothermal technique has been proved to be fruitful to achieve changeable morphologies, which serves as the precursor of nanostructured-Co_3O_4 to produce specific morphology. However, the high-pressure needed in preparation limits the application Co_3O_4 in LIBs.

Recently, low temperature refluxing is a simple route in an open system to prepare porous transition metal oxides. Refluxing technique will be a good way to control the decomposition of aqueous urea and to produce metal oxides with tunable morphologies. Herein, we report the synthesis of the self-assembly cobalt hydrotalcite-like compounds (Co-HLC) through refluxing the mixture of cobaltous nitrate and urea. Along with the increased refluxing temperature, the precursors of Co-HLCs change from nanoleafs to nanosheets structure. After pyrolysis, the specific morphology is successfully maintained in the final product of Co_3O_4 which the samples assembled by ordered nanosheets has stable porous structure during lithiation/delithiation and good contact with electrolyte. The as-prepared porous Co_3O_4 samples are evaluated as anode materials for LIBs in detail.

2 . Experimental

All experiments were carried in a 200 mL flasks equipped with an Allihn condenser. 4 g of $Co(NO_3)_2{\cdot}6H_2O$ and 3.5 g of urea were dissolved in 100 mL of ethanol/water (1:1) solution under vigorous stirring for 30 min. The mixture was refluxed for 12 h. After cooling down to room temperature, the solution was

centrifuged at 5000 rpm. The precipitate was washed for several times, and dried at 60 °C in vacuum. The produced Co-hydrotalcite-like compounds (Co-HLC) were simply named as Co-HLC-90, Co-HLC-120 and Co-HLC-150 according to the refluxing temperature of 90, 120 and 150 °C respectively. Co-HLCs were pyrolysis in Muffle furnace at 350 °C for 3 h under air atmosphere. The heating rate is controlled at 1° min^{-1}. The as-synthesized metal oxides are simply named as Co_3O_4-90, Co_3O_4-120 and Co_3O_4-150, respectively.

X-ray studies were done in the 2θ range of 10-80° and scan rate of 4° min^{-1} by powder X-ray diffractmeter (XRD, Rigaku, Cu-Kα radiation at 30 kV and 30 mA, λ=1.5418 A□). FT-IR spectra of KBr powder pressed pellets were recorded on a Bruker VECTOR 22 spectrometer. The crystal morphology was characterized by using field emission scanning electron microscope (FESEM, Zeiss Sigma microscope, 20kV), and transmission electron microscope (TEM, JEOL-2000CX, 200 kV). Specific surface areas were estimated by N_2 adsorption–desorption isotherms at 77 K (Micromeritics ASAP 2020) by using the BET (Brunauer−Emmet−Teller) method. The C, H, N compositions of Co-HLCs were measured by VarioEL III elemental analyzer (Elementar, Germany). Thermogravimetric analysis (TGA) and differential scanning calorimeter (DSC) of the samples were recorded in a TG-DSC thermal analyzer system (STA449F3, NETZSCH).

The electrochemical measurements were carried out using CR2016 coin-type cell. The composite cathode was formulated with active materials, conductive Super P and poly (vinylidene fluoride) (weight ratio of 8:1:1) mixed in N-methyl-2-pyrrolidone. After stirred for 2 h, the slurry was cast onto Cu foil by using a doctor blade. The film was dried under vacuum at 120 °C for 6 h. The mass loading of active material in electrodes is about 3 mg cm^{-2}. The coin cells were assembled in an argon-filled glove

box, using lithium metal as the negative electrode, Celgard 2500 as the separator, and 1 M $LiPF_6$ dissolved in ethylene carbonate, dimethyl carbonate and ethyl-methyl carbonate (1:1:1 by volume) as the electrolyte. The galvanostatic charge and discharge test was recorded on LAND battery program control testing system (CT2001A, Wuhan, China). The cut-off voltage is range of 0.001-3.0 V. Cyclic voltammetry (CV) was recorded on an electrochemical workstation (PARSTAT2273, Princeton Applied Research, USA) at the scanning rate of 0.1 mV s^{-1} between the potential ranges of 0 and 3.0 V. The capacitance was measured in a three-electrode system containing a platinum sheet as a counter electrode, saturated calomel electrode as reference, and the product as the working electrode. The electrolyte is an aqueous solution of 1 M H2SO4. The supercapacitor performance was measured by CVs (PARSTAT2273 electrochemical workstation, Princeton Applied Research, USA) and galvanostatic charge–discharge system (LAND CT2001A, Wuhan, China) in the voltage range from 0 V to 1.0 V. Different sweep rates (5, 10, 20, 50, and 100 mV s^{-1}) and current densities (0.5–20 A g^{-1}) were employed, respectively.

3 . Results and Discussions

Fig. 1 shows the proposed morphology evolution controlled by refluxing temperature. Cobaltous nitrate and urea are dissolved in ethanol/water (1:1) at first, and the mixture was refluxed for 12 h. It includes two stages, decomposition of urea and Co-HLC growth. Beyond 80 °C, the in-situ decomposition of the aqueous urea releases precipitating ligands (OH^- and CO_3^{2-}) into the reaction system [36]. The cobaltous is expected to form hydroxide, and thus the nitrate and carbonate incorporation can take place in intercalation the brucite-like layer. The adjustable refluxing temperature plays the key factor controlling the nucleation and growth of

the Co-HLC precipitates, that is, the specific morphologies of Co-HLC will be facilely controlled (as shown Fig. 1) from nanowire to nanosheets. The higher refluxing temperature used improves the crystal growth of Co_3O_4 on two-dimensional direction.

The SEM images of Co-HLCs and Co_3O_4 are also shown in Fig. 1. The overall morphologies of Co-HLCs are micro-spherical shape, which self-assembly grow through a primary crystal as the center. During the growth of Co-HLCs under refluxing situation, the sample towards their own preferential growth behavior under various refluxing situation. Under refluxing temperature of 90 °C, fibrous structure prefers to grow in two-dimensional direction based on the nuclei, and finally the nanoleafs structure is formed (Fig. 1a). At the moderate refluxing temperature of 120 °C, the growth of nuclei toward the two-dimensional direction and nanosheets is grown. These multiple layers of nanosheets are connected to each other through the center to form three-dimensional flower-like porous structure (Fig. 1b). At the highest refluxing temperature of 150 °C, cabbage-like structure is grown because the nanoleafs are rapidly grown and toward intensely amassed (Fig. 1c). After a thermal treatment, no apparent collapses of Co-HLCs are observed and the original morphologies of the precursors are perfectly retained, except that there are numerous pores appear. For example, Co-HLC-90 remains the fibrous structure assembled by Co_3O_4 crystallites (Fig. 1a'). The Co-HLC-150 converts to a compact cabbage-like structure, which each nanoleafs are composed by Co_3O_4 crystallites too (Fig. 1c'). Co-HLC-120 converts to relatively ordered and porous nanosheets, which is very important in the electrochemical properties.

Fig. 2a shows the XRD patterns of intermediates of Co-HLCs. The samples obtained at various refluxing temperatures present the almost same peak positions and

intensities. It clearly indicates that the diffraction peaks are similar with those of metal HLCs reported in the literatures [36-38]. The as-produced Co-HLCs maybe expressed by a general formula of $M_x(OH)_y(X)_z \cdot nH_2O$ (M: metal; X: anions). In comparison with the basic structure of brucite, the inter-hydrotalcite-like layered distance of Co-HLCs is increased to 7.16 Å, due to the intercalation of nitrate and carbonate anions. The infrared spectra of the Co-HLCs are shown in Fig. 2b. The absorption peak near 3629 cm^{-1} is attributed to the stretching vibration of O-H. The strong peak at 2233 cm^{-1} can be assigned to the stretching vibration of CO=N species that is the evidence of the existence of the intercalated ions of CON^- in the interlayers of Co-HLCs. Bands of N-O in C_{2v} symmetry are observed at 1383 and 1289 cm^{-1} which come from the anions of NO^{3-} intercalated in the interlayered space of Co-HLCs. The sharp absorption peak at 1486 cm^{-1} can be assigned to the CO_3^{2-} anion in the interlayer space and the adsorption band observed at 1629 cm^{-1} can be assigned to the molecular vibrations of the interlayered water in Co-HLCs [39]. The strong and widen peak around 636 cm^{-1} is attributed to the stretching vibration of Co-O bond.

The three samples of Co-HLCs present similar TG/DSC profiles in Fig. 3. Before 100 °C, there is an endothermic peak and weigh loss about 2%*wt*, corresponding to the removal of apparent water absorbed in the environment. Most of the decomposition of Co-HLCs appears at 230-250 °C corresponding to a sharp exothermic peak. The weight losses in this stage are 25.50, 23.94 and 27.22 %*wt* of Co-HLC-90, Co-HLC-120 and Co-HLC-150, respectively, which comes from the removal of hydroxyl, nitrate and carbonate anions in the samples. Table 1 lists the elemental results of C, H and N of Co-HLCs. The atomic ratios of C, N and H elements are minor deviated values, because the amount of the intercalated CO_3^{2-} and NO_3^- anions in Co-HLCs is dependent on the refluxing temperature. For example,

Co-HLC-90 has the lowest ratio of carbon, Co-HLC-120 contains the lowest nitrogen element. Co-HLC-150 has the highest weight ratio of C, N and H, corresponding to the highest weight loss of 27.22% shown in Fig. 3c. It can be proposed that the amount of the intercalated CO_3^{2-} and NO_3^- anions in brucite structure are dependent on the refluxing temperatures. According to the results of TGA, FTIR and elemental analysis, it can be concluded the composition of Co-HLCs is $Co(CO_3)_{0.28\text{-}0.3}(NO_3)_{0.96\text{-}1.15}(OH)_{0.26\text{-}0.29}$. After 320 ℃, there is none weight loss of Co-HLCs except the thermal changing till 500 °C, this period should correspond to the growth of Co_3O_4. That is why the calcination temperature is 350 °C for 3 h to assure the crystallization of Co_3O_4.

Co-HLCs are decomposed and Co_3O_4 nanoparticles are simultaneously grown under 350 °C in air atmosphere. The crystal morphologies of Co_3O_4 almost maintain the original structure of Co-HLCs accompanying the slowly removal of small molecules. The obtained Co_3O_4 powders are black in color. Fig. 4 shows the XRD patterns and crystallites morphologies of Co_3O_4 samples. All the peaks are index to a pure face-centered-cubic phase of Co_3O_4 (JCPDS No. 42-1467, space group: Fd3m, a = 8.065 Å). No impurity phase of other cobalt oxides can be found. Co_3O_4-90, Co_3O_4-120 and Co_3O_4-150 samples are the primary nanoparticles that are homogeneous with an average crystal size about 50 nm.

The specific surface areas of Co_3O_4-90, Co_3O_4-120 and Co_3O_4-150 are measured by Brunauer-Emmett-Teller (BET). The nitrogen adsorption/desorption isotherms at 77 K of Co_3O_4-90, Co_3O_4-120, and Co_3O_4-50 are shown in Fig. 5 and the insets are pore size distributions of the relative samples by Barrett-Joyner-Halenda (BJH) method. The specific surface area of Co_3O_4-90, Co_3O_4-120, and Co_3O_4-150 are calculated to be 17.0, 22.4 and 24.9 m2 g^{-1}, respectively. The isotherm of the three

samples is type IV with a typical H3 hysteresis loop, that is accordance with the Co_3O_4 samples composed by aggregated structure with slit-like pores found in the previous SEM images (in Fig. 1). The small loops varying about from P/P_0 0.94 to 1.0 are assigned to interparticle porosity due to agglomeration of the nanosheets in the three samples. Co_3O_4-90 with fibrous structure assembled by crystallites give a narrow pore-size distribution, while Co_3O_4-120 and Co_3O_4-150 give majority pores near 2 nm. The small pore-size attributed to the interparticle porosity produced by the decomposition of the intermediates of Co-HLCs. Co_3O_4-120 and Co_3O_4-150 give minority mesopores due to the interstitial space between the nanoflakes as observed by the SEM images (Fig. 1).

Fig. 6 shows the cyclic voltammograms (CV) of Co_3O_4 samples recorded at a scan rate of 0.1 mV s^{-1}. Co_3O_4-90, Co_3O_4-120 and Co_3O_4-150 present the initial electrochemical response as shown a pair of well-defined redox peaks at 2.07/1.00 V, 2.07/1.01 V and 2.00/1.00 V, respectively. In the following two CV cycles, the redox peaks of Co_3O_4-150 shift to much higher value in anodic process and to much lower value in cathodic process accompany with the peak current decreases (as shown in Fig. 6c). It indicates a slower response and weaker reversibility of Li^+ than that of Co_3O_4-90 and Co_3O_4-120, because the porous and open structure in Co_3O_4-90 and Co_3O_4-120 provide the channel of lithium diffusion during redox processes. Potential difference of redox peaks, ΔE, is always representative of the kinetic process, especially considering that the electrochemical process involves lithium diffusion in a solid phase and electron jumping across the electrode. Considering the crystal morphologies of the as-synthesized samples, Co_3O_4-150 produced under high temperature of hydrothermal condition presents close packed nanosheets compared with Co_3O_4-90 and Co_3O_4-120 they have a relatively loosen structure. After several

redox cycles, the close packed structure in Co_3O_4-150 suffers worsen collapsed accompany with the phase change of Co_3O_4 during lithiation/delithiation,.

To study the performance of the as-synthesized Co_3O_4 with various morphologies and structure, galvanostatic charge-discharge are performed using half-battery of Co_3O_4/Li metal. Fig. 7 shows the initial charge/discharge profiles and cyclic performance of the three samples at the current density of 100 mA g^{-1}. Co_3O_4 as anode shows low potential for LIBs and higher specific capacity than commercial graphite. The three samples shows a clear potential plateau around ~1.0 V vs Li^+/Li at the initial discharge curve and a sloping tail to 0.001 V. In the higher-voltage region, only one voltage plateau at 1.05 V is observed in Co_3O_4-120, but two voltage plateaus at 1.05 V and 1.2 V are observed in Co_3O_4-90 and Co_3O_4-150. The two voltage plateaus in Co_3O_4-90 and Co_3O_4-150 can be attributed to the conversion from Co_3O_4 to an intermediate phase of CoO at 1.2 V and then to metallic Co at 1.05 V, respectively [40,41]. Co_3O_4-120 with single and direct conversion from Co_3O_4 to metallic Co is conducive to the best electrochemical performance. As shown in Fig. 7a, the initial discharge capacity of Co_3O_4-90, Co_3O_4-120 and Co_3O_4-150 are 1015, 1008 and 1089 mAh g^{-1}, respectively. All of these values are higher than the theoretical capacity of Co_3O_4 (890 mAh g^{-1}). This is always ascribed to the irreversible reactions to form a solid electrolyte interphase film (SEI) and possibly interfacial lithium storage [40,41]. The following charge capacities of Co_3O_4-90, Co_3O_4-120 and Co_3O_4-150 are down to 691, 722 and 386 mAh g^{-1}, respectively. After 100 cycles, the reversible capacities of Co_3O_4-90, Co_3O_4-120, Co_3O_4-150 are 558, 743 and 415 mAh g^{-1}, respectively. As expected, the cyclic performance of the Co_3O_4-120 with flower-like morphology is substantially better than that of Co_3O_4-90 (porous nanoleafs) and Co_3O_4-150 (compact nanoleafs).

Because the capacity of LIB always depends on the electrode materials synthesized in various conditions, the sample with porous structure and large surface area would display higher reversible capacities that exceeded theoretical capacity because Li^+ ions stored in the interfaces and pores of the porous material could take part in the reaction [29, 40]. In this work, the reflux temperature is just one of the factors affecting the morphology and microstructure of Co_3O_4 which really impacts the relative electrochemical performance. A proper refluxing temperature ensures the product with an optimum particle size and crystal morphologies, and hence the best electrochemical performance. Co_3O_4 as anode material reveals the electrochemical reactions in Co_3O_4/Li battery as follows [42]:

Cathode: $Co_3O_4 + 8\ Li^+ + 8\ e^- \Leftrightarrow 3\ Co + 4\ Li_2O$ (Eq. 1)

Anode: $8\ Li - 8\ e^- \Leftrightarrow 8\ Li^+$ (Eq. 2)

Overall reaction: $Co_3O_4 + 8\ Li^+ \Leftrightarrow 3\ Co + 4\ Li_2O$ (Eq. 3)

During the discharge process the metallic cobalt and Li_2O are formed, and then in the following charge step metallic particles of cobalt decomposes Li_2O to form Co_3O_4 again. The conductivity and stability of the nanostructure of Co_3O_4 sample are the important factors in the capacity and cyclic performance. Stable Co_3O_4 structure can maintain the nanosized crystallite of metallic cobalt and activate the decomposition of Li_2O, thus conducive to maintaining the stability of the capacity as well. In this work, Co-HLC-120 as template in pyrolysis at 350 °C provides the framework of flower-like structure. The opened and porous structure of Co_3O_4-120 provides good contact with electrolyte, lower polarization and stable crystal structure for Li^+ involved in lithiation/delithiation.

The rate performance of anode materials is another important factor in practical application. Fig. 8 shows the cyclic performance of Co_3O_4 as anode worked under

various current densities. The discharge plateaus of the three samples are towards the low values along with the increased current densities (Fig. 8a-8c). In comparison with the relative poor capacities presented in Co_3O_4-90 and Co_3O_4-150, the electrode of Co_3O_4-120 demonstrates the best rate performance. As shown in Fig. 8d, Co_3O_4-120 electrode deliver 796, 732 and 648 mAh g^{-1} at 40, 400 and 1500 mA g^{-1}, respectively. When the rate returns back to 40 mA g-1, Co_3O_4-120 can retain the high specific capacity of 785 mAh g^{-1}. The excellent rate performance of Co_3O_4-120 should be attributed to the porous and homogeneous overlapping structure assuring the good contact between active materials of Co_3O_4 and electrolyte. However, Co_3O_4-150 with close packed structure cannot provide efficient conductivity, and thus the poorest rate performance presents in Fig. 8f. Under 1500 mA g^{-1}, the discharge capacity of Co_3O_4-150 electrode almost drops to zero, and Co_3O_4-150 electrode only retain 270 mAh g^{-1} when it works under the rate 40 mA g^{-1} again.

Fig. 9 presents the long cyclic performance at the current density of 800 mA g^{-1}. Co_3O_4-90, Co_3O_4-120 and Co_3O_4-150 as electrodes release the initial capacities of 545, 756 and 617 mAh g^{-1}, and presents the following charge capacities of 370, 690, and 533 mAh g^{-1}, respectively. Co_3O_4-120 maintains good cyclic performance, 587 mAh g^{-1} at the 100th cycle, but Co_3O_4-150 appears rapid capacity fading due to the irreversible processes of lithiation/delithiation of Co_3O_4, only 46 mAh g^{-1} at the 100th cycle. A reasonable explanation is that electrolyte can efficiently migrates through the porous active materials by capillary action. During the metal cobalt and Li_2O are formed in discharge, and metal particles of cobalt decomposes Li_2O to form Co_3O_4 again in charge, irreversible crystal morphology happens more and more seriously in Co_3O_4-150. The compact and aggregated nanoleafs of Co_3O_4-150 hinders the

diffusion of lithium ions toward the inside during lithiation/delithiation processes. The compact structure of Co_3O_4-150 results in the fact that the particles are aggregated and the electrolyte may not fill in them, that is, only a part of Co_3O_4 as active material involve in lithiation/delithiation. Based on the above electrochemical analysis, reversible and porous structure in Co_3O_4-120 rather than an optimum crystal size assures its enhanced electrochemical performance.

To further explore the potential applications in energy storage, Co_3O_4-120 were fabricated into supercapacitor electrodes and characterized by CV and galvanostatic charge/discharge measurements. Fig. 10a presents typical CV curves of Co_3O_4-120 at various sweeping rates. The CV curve recorded at low scan rate is symmetrical rectangular-shape with minor redox peaks. It is an evident that Co_3O_4-120 electrode demonstrates pseudo-capacitive properties. The peak current increases with a significant change in CVs shape when scan rates increase from 5 to 100 mV s^{-1}, which is attributed a good electrochemical reversibility and high power characteristics of Co_3O_4-120 electrode. Fig. 10b shows the galvanostatic charge/discharge curves and cyclic capacitance at current density of 1 A g^{-1}. Co_3O_4-120 electrode presents excellent cyclic performance and delivers 167 F g^{-1} after 3000 cycles. At various current densities, Co_3O_4-120 electrode still delivers excellent capacitances, for example, 128, 104 and 90 F g^{-1} of Co_3O_4-120 electrode carried out under the current densities of 5, 10 and 20 A g^{-1}.

4. Conclusions

Refluxing method was widely used as one of the simple synthetic routes for nano-sized samples. Refluxing is a good way to control the decomposition of aqueous urea. In this work, the self-assembly cobalt hydrotalcite-like compounds (Co-HLC)

was synthesized through refluxing the mixture of cobaltous nitrate and urea. Along with the increased refluxing temperature, the precursors of Co-HLCs changed from porous to close packed structure. During pyrolysis, Co-HLCs were decomposed and Co_3O_4 nanoparticles were simultaneously grown. The specific morphology was successfully maintained in the final product of Co_3O_4 which Co_3O_4-120 assembled by ordered nanosheets were stable porous structure during lithiation/delithiation and good contact with electrolyte. Co_3O_4-120 showed the charge capacities of 720 and 737 mAh g^{-1} at the 2nd and 100th cycle under the current density of 100 mA g^{-1}. At the current density of 800 mA g^{-1}, Co_3O_4-120 as electrodes released the initial capacities of 756 mAh g^{-1}, and remained 582 mAh g^{-1} at the 100th cycle. The reversible and porous structure in Co_3O_4-120 rather than an optimum crystal size assure its enhanced electrochemical performance. The porous structure also contributes to excellent capacitance in Co_3O_4-120 as electrode for a supercapacitor. In conclusion, the efficient route of refluxing could be used to prepare other porous transition metal oxides as anode materials for LIBs.

Acknowledgements

This work was supported by National Natural Science Foundation of China (Grant No. 51172032) and Natural Science Foundation of Jiangsu Province of China (Grant No. BK20141229) and NSF of FP7 Marie Curie Action sponsored by European Commission (Project No. 295208).

References

[1] D. Larcher, J. M. Tarascon, Towards greener and more sustainable batteries for electrical energy storage, Nat. Chem. 7 (2015) 19-29.

[2] B. Scrosati, J. Hassoun, Y. K. Sun, Lithium-ion batteries. A look into the future, Energ. Environ. Sci. 4 (2011) 3287.

[3] J. R. Dahn, A. K. Sleigh, H. Shi, J. N. Reimers, Q. Zhong, B. M. Way, Dependence of the electrochemical intercalation of lithium in carbons on the crystal structure of the carbon, Electrochim. Acta 38 (1993) 1179-1191.

[4] K. Sawai, Y. Iwakoshi, T. Ohzuku, Carbon materials for lithium-ion (shuttlecock) cells, Solid State Ionics 69 (1994) 273-283.

[5] H.H. Zhang, X.H. Li, H.J. Guo, Z.X. Wang, Y. Zhou. Hollow Si/C composite as anode material for high performance lithium-ion battery, Powder Technol. 299 (2016) 178–184.

[6] H. Y. Wang, H. Q. Huang, L. Chen, C. G. Wang, B. Yan, Y. T. Yu, Y. Yang, G. Yang, Preparation of Si/Sn-based nanoparticles composited with carbon fibers and improved electrochemical performance as anode materials, ACS Sustainable Chem. Eng. 2 (2014) 2310−2317.

[7] F. Wang, L. Chen, C. Deng, H. Ye, X. Jiang, G. Yang, Porous tin film synthesized by electrodeposition and the electrochemical performance for lithium-ion batteries, Electrochim. Acta 149 (2014) 330-336.

[8] J. Hassoun, G. Derrien, S. Panero, B. Scrosati, A nanostructured Sn-C composite lithium battery electrode with unique stability and high electrochemical Performance, Adv. Mater. 20 (2008) 3169-3175.

[9] H. Y. Wang, P. Gao, S. F. Lu, H. D. Liu, G. Yang, J. Pinto, X. F. Jiang, The effect of tin content to the morphology of Sn/Carbon nanofiber and the electrochemical

performance as anode material for lithium batteries, Electrochim. Acta 58 (2011) 44-51.

[10] W. X. Chen, J. Y. Lee, Z. Liu, The nanocomposites of carbon nanotube with Sb and $SnSb_{0.5}$ as Li-ion battery anodes, Carbon 41 (2003) 959-966.

[11] M. N. Obrovac, V. L. Chevrier, Alloy negative electrodes for Li-ion batteries, Chem. Rev. 114 (2014) 11444-502.

[12] T. Wang, S.J. Shi, F.J. Kong, G. Yang, B. Qian, F. Yin, The role of stable interface in nano-sized $FeNbO_4$ as anode electrode for lithium-ion batteries, Electrochimica Acta 203 (2016) 206-212.

[13] L. Pan, K.-X. Wang, X.-D. Zhu, X.-M. Xie, Y.-T. Liu, Hierarchical assembly of SnO2 nanowires on MnO2 nanosheets: a novel 1/2D hybrid architecture for high-capacity, reversible lithium storage. J. Mater. Chem. A 3 (2015) 6477-6483.

[14] K. Zhang, X. Han, Z. Hu, X. Zhang, Z. Tao, J. Chen, Nanostructured Mn-based oxides for electrochemical energy storage and conversion, Chem. Soc. Rev. 44 (2015) 699-728.

[15] M. V. Reddy, G. V. Subba Rao, B. V. Chowdari, Metal oxides and oxysalts as anode materials for Li ion batteries, Chem. Rev. 113 (2013) 5364-457.

[16] D. J. Yan, X. D. Zhu, K. X. Wang, X. T. Gao, Y. J. Feng, K. N. Sun, Y. T. Liu. Facile and elegant self-organization of Ag nanoparticles and TiO_2 nanorods on V_2O_5 nanosheets as a superior cathode material for lithium-ion batteries. J. Mater. Chem. A 4 (2016) 4900-4907

[17] C. Ban, Z. Wu, D. T. Gillaspie, L. Chen, Y. Yan, J. L. Blackburn, A. C. Dillon, Nanostructured Fe_3O_4/SWNT electrode: Binder-free and high-rate li-ion anode, Adv. Mater. 22 (2010) E145-9.

[18] G. Yang, Y. Li, H. Ji, H. Wang, P. Gao, L. Wang, H. Liu, J. Pinto, X. Jiang,

Influence of Mn content on the morphology and improved electrochemical properties of Mn_3O_4|MnO@carbon nanofiber as anode material for lithium batteries, J. Power Sources 216 (2012) 353-362.

[19] B. Varghese, M. V. Reddy, Z. Yanwu, C. S. Lit, T. C. Hoong, G. V. Subba Rao, B. V. R. Chowdari, A. T. S. Wee, C. T. Lim, C. Sow, Fabrication of NiO nanowall electrodes for high performance lithium ion battery, Chem. Mater. 20 (2008) 3360-3367.

[20] J. Wang, Q. Zhang, X. Li, B. Zhang, L. Mai, K. Zhang, Smart construction of three-dimensional hierarchical tubular transition metal oxide core/shell heterostructures with high-capacity and long-cycle-life lithium stroage. Nano Energy 12 (2015) 437-446.

[21] T. Li, X. Li, Z. Wang, H. Guo, Y. Li, A novel $NiCo_2O_4$ anode morphology for lithium-ion batteries, J. Mater. Chem. A, 3 (2015) 11970.

[22] Q. Zhang, J. Wang, J. Dong, F. Ding, X. Li, B. Zhang, S. Yang, K. Zhang, Facile general strategy toward hierarchical mesoporous transition metal oxides arrays on three-dimensional macroporou foam with superior lithium storage properties. Nano Energy 13 (2015) 77-91.

[23] N. Jayaprakash, W. D. Jones, S. S. Moganty, L. A. Archer, Composite lithium battery anodes based on carbon@Co_3O_4 nanostructures: Synthesis and characterization, J. Power Sources 200 (2012) 53-58.

[24] H. Wu, M. Xu, Y. Wang, G. Zheng, Branched Co_3O_4/Fe_2O_3 nanowires as high capacity lithium-ion battery anodes, Nano Res. 6 (2013) 167-173.

[25] J. Wang, N. Yang, H. Tang, Z. Dong, Q. Jin, M. Yang, D. Kisailus, H. Zhao, Z. Tang, D. Wang, Accurate control of multishelled Co_3O_4 hollow microspheres as high-performance anode materials in lithium-ion batteries, Angew. Chem. Int. Ed. 52

(2013) 6417-20.

[26] X. Rui, H. Tan, D. Sim, W. Liu, C. Xu, H. H. Hng, R. Yazami, T. M. Lim, Q. Yan, Template-free synthesis of urchin-like Co_3O_4 hollow spheres with good lithium storage properties, J. Power Sources 222 (2013) 97-102.

[27] X. Wang, X. L. Wu, Y. G. Guo, Y. Zhong, X. Cao, Y. Ma, J. Yao, Synthesis and Lithium Storage Properties of Co_3O_4 Nanosheet-Assembled Multishelled Hollow Spheres, Adv. Funct. Mater. 20 (2010) 1680-1686.

[28] J. Zhu, L. Bai, Y. Sun, X. Zhang, Q. Li, B. Cao, W. Yan, Y. Xie, Topochemical transformation route to atomically thick Co_3O_4 nanosheets realizing enhanced lithium storage performance, Nanoscale 5 (2013) 5241-6.

[29] M. Y. Son, Y. J. Hong, Y. C. Kang, Superior electrochemical properties of Co_3O_4 yolk-shell powders with a filled core and multishells prepared by a one-pot spray pyrolysis, Chem. Comm. 49 (2013) 5678-80.

[30] M. Xu, F. Wang, M. Zhao, S. Yang, X. Song, Molten hydroxides synthesis of hierarchical cobalt oxide nanostructure and its application as anode material for lithium ion batteries, Electrochim. Acta 56 (2011) 4876-4881.

[31] M. Cuglietta, K.L. Chaudhary, S.Q. Ge, O. Kesler. Development of a multi-component aqueous NiO, CuO, and Co_3O_4 suspension for use in suspension plasma spraying of SOFC anode layers. Powder Technol. 237 (2013) 76–86.

[32] L. Man, B. Niu, H. Xu, B. Cao, J. Wang, Microwave hydrothermal synthesis of nanoporous cobalt oxides and their gas sensing properties, Mater. Res. Bull. 46 (2011) 1097-1101.

[33] J. Deng, L. Zhang, H. Dai, Y. Xia, H. Jiang, H. Zhang, H. He, Ultrasound-assisted nanocasting fabrication of ordered mesoporous MnO_2 and Co_3O_4 with high surface areas and polycrystalline walls, J. Phys. Chem. C 114 (2010)

2694-2700.

[34] W. Wang, J. Xu, Structure and visible light luminescence of 3D flower-like Co_3O_4 hierarchical microstructures assembled by hexagonal porous nanoplates, ACS Appl. Mater. Interfaces 7 (2015) 415-21.

[35] J.P. Robinson, G.M. Koenig Jr. Tuning solution chemistry for morphology control of lithium-ion battery precursor particles. Powder Technol. 284 (2015) 225–230.

[36] R. Xu, H. C. Zeng, Synthesis of Nanosize Supported Hydrotalcite-like Compounds $CoAl_x(OH)_{2+2x}(CO_3)_y(NO_3)_{x-2y}\cdot nH_2O$ on γ-Al_2O_3, Chem. mater. 13 (2010) 297-303.

[37] Y. Ding, L. Xu, C. Chen, X. Shen, S. L. Suib, Syntheses of nanostructures of cobalt hydrotalcite like compounds and Co_3O_4 via a microwave-assisted reflux method, J. Phys. Chem. C 112 (2008) 8177-8183.

[38] T. Nygil, R. Michael, High selectivity in anion exchange reactions of the anionic clay, cobalt hydroxynitrate, J. Mater. Chem. A J 21 (2011) 18077.

[39] M. Rajamathi, P. V. Kamath, Urea hydrolysis of cobalt(II) nitrate melts: synthesis of novel hydroxides and hydroxynitrates, Int. J. Inorg. Mater. 3 (2001) 901-906.

[40] N. Yan, L. Hu, Y. Li, Y. Wang, H. Zhong, X. Hu, X. Kong, Q. Chen, Co_3O_4 Nanocages for High-Performance Anode Material in Lithium-Ion Batteries, J. Phys. Chem. C 116 (2012) 7227-7235.

[41] W. Y. Li, L. N. Xu, J. Chen, Co_3O_4 nanomaterials in lithium-ion batteries and gas sensors, Adv. Funct. Mater. 15 (2005) 851-857.

[42] S. L. Chou, J. Z. Wang, H. K. Liu, S. X. Dou, Electrochemical deposition of porous Co_3O_4 nanostructured thin film for lithium-ion battery, J. Power Sources 182 (2008) 359-364.

Table 1 Elemental analysis of Co-intermediates synthesized under various refluxing temperatures.

sample	experimental atomic ratio (wt%)			calculated atomic ratio (wt%)		
	C	N	H	C	N	H
Co-HLC-90	6.82	7.34	1.92	0.57	0.52	1.92
Co-HLC-120	6.93	6.57	2.14	0.58	0.47	2.14
Co-HLC-150	7.22	8.13	2.30	0.60	0.58	2.30

Figure Captions

Fig. 1 Schematic preparation route for the Co-HLCs and Co_3O_4. SEM images of (a) Co-HLC-90 and (a') Co_3O_4-90, (b) Co-HLC-120 and (b') Co_3O_4-120, and (c) Co-HLC-150 and (c') Co_3O_4-150, respectively.

Fig. 2 XRD patterns (a) and FTIR spectra (b) of Co-HLCs refluxed at 90 °C, 120 °C and 150 °C, respectively.

Fig. 3 TGA/DSC curves of Co-HLC-90 (a), Co-HLC-120 (b), and Co-HLC-150 (c).

Fig. 4 XRD patterns and TEM images of Co_3O_4-90, Co_3O_4-120, and Co_3O_4-150, respectively.

Fig. 5 N_2 adsorption−desorption isotherm of (a) Co_3O_4-90, (b) Co_3O_4-120, and (c) Co_3O_4-150. The inset in each isotherm is the corresponding pore size distributions.

Fig. 6 The first three CV curves of (a) Co_3O_4-90, (b) Co_3O_4-120 and (c) Co_3O_4-150 at a scan rate 0.1 mV s^{-1}.

Fig. 7 The first charge-discharge cycles (a) and cycle performance (b) of the Co_3O_4 at the current density of 100 mA g^{-1}.

Fig. 8 The initial charge/discharge curves and rate performance of Co_3O_4-90 (a) and (b), Co_3O_4-120 (c) and (d), Co_3O_4-150 (e) and (f) carried out at various current densities.

Fig. 9 The cyclic performance of Co_3O_4-90 (a), Co_3O_4-120 (b), Co_3O_4-150 (c) as anode worked at the current density of 800 mA g^{-1}.

Fig. 10 The electrochemical performance of Co_3O_4-120 as electrode in a supercapacitor. The CV curves of Co_3O_4-120 electrode v.s. Hg/Hg_2Cl_2 carried out under various scanning rates (a). Cyclic supercapacitance and galvanostatic charge-discharge curves at 1 A g^{-1} (b). Rate performance of Co_3O_4-120 electrode at different current densities from 0.5 A g^{-1} to 20 A g^{-1}.

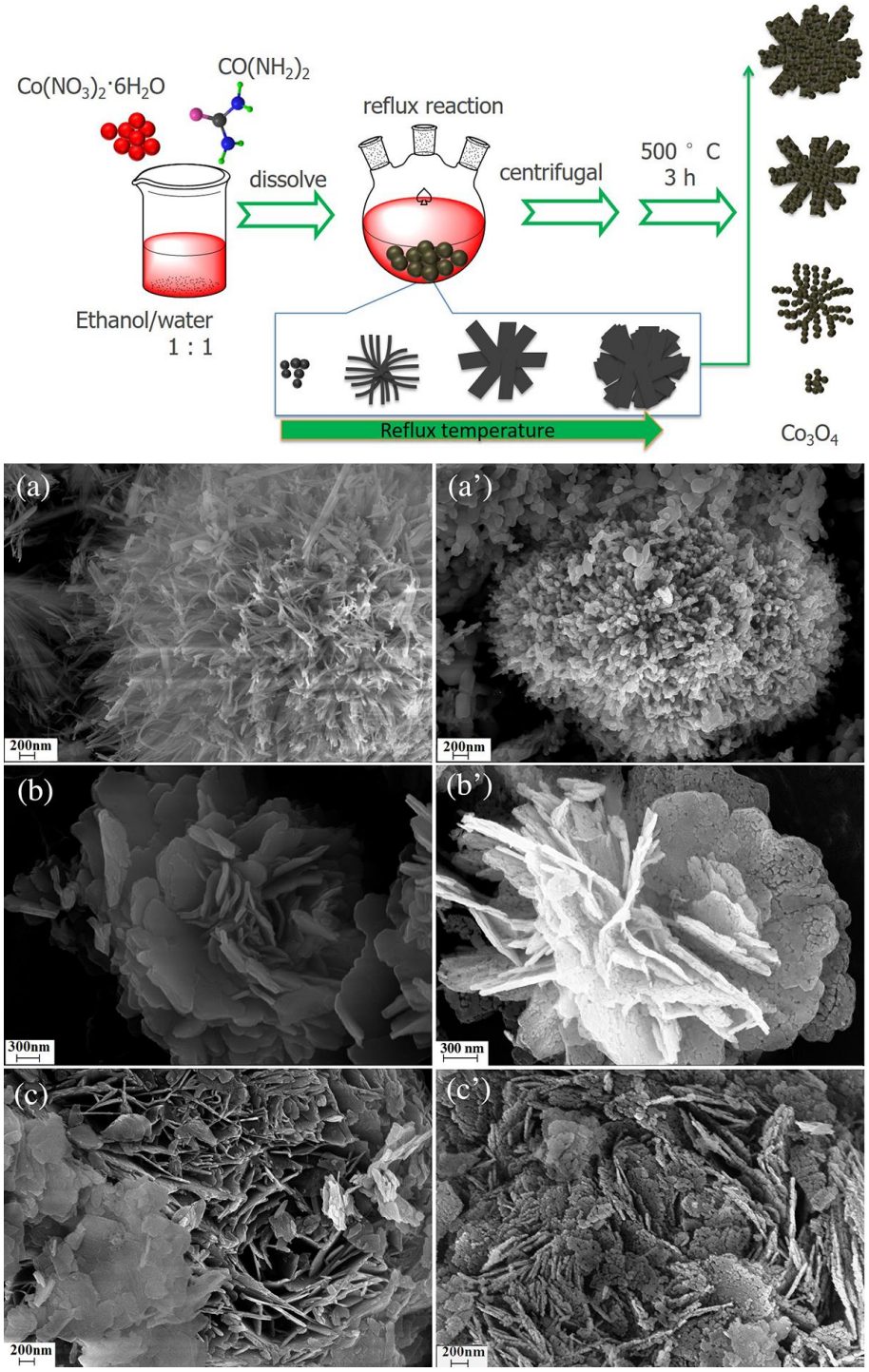

Fig. 1 Schematic preparation route for the Co-HLCs and Co_3O_4. SEM images of (a) Co-HLC-90 and (a') Co_3O_4-90, (b) Co-HLC-120 and (b') Co_3O_4-120, and (c) Co-HLC-150 and (c') Co_3O_4-150, respectively.

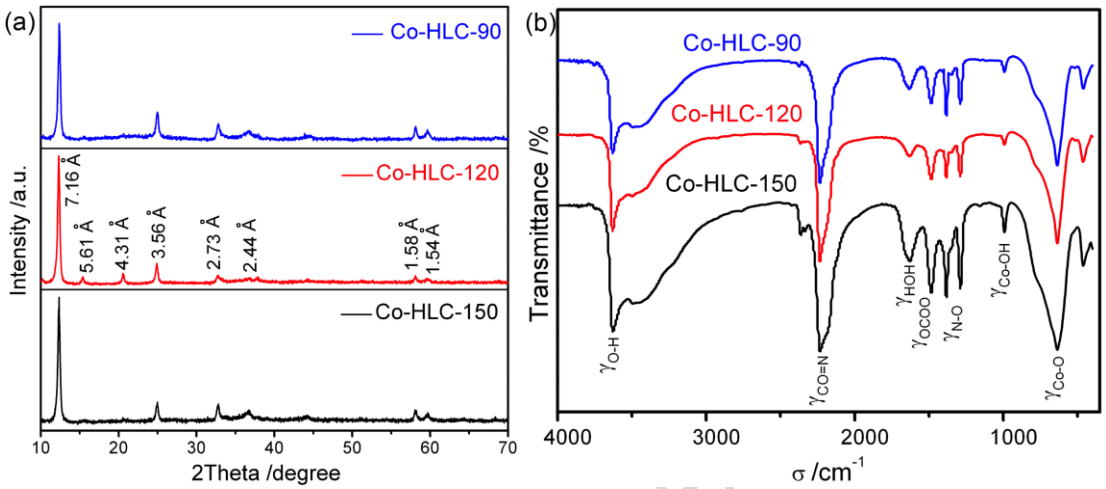

Fig. 2 XRD patterns (a) and FTIR spectra (b) of Co-HLCs refluxed at 90 °C, 120 °C and 150 °C, respectively.

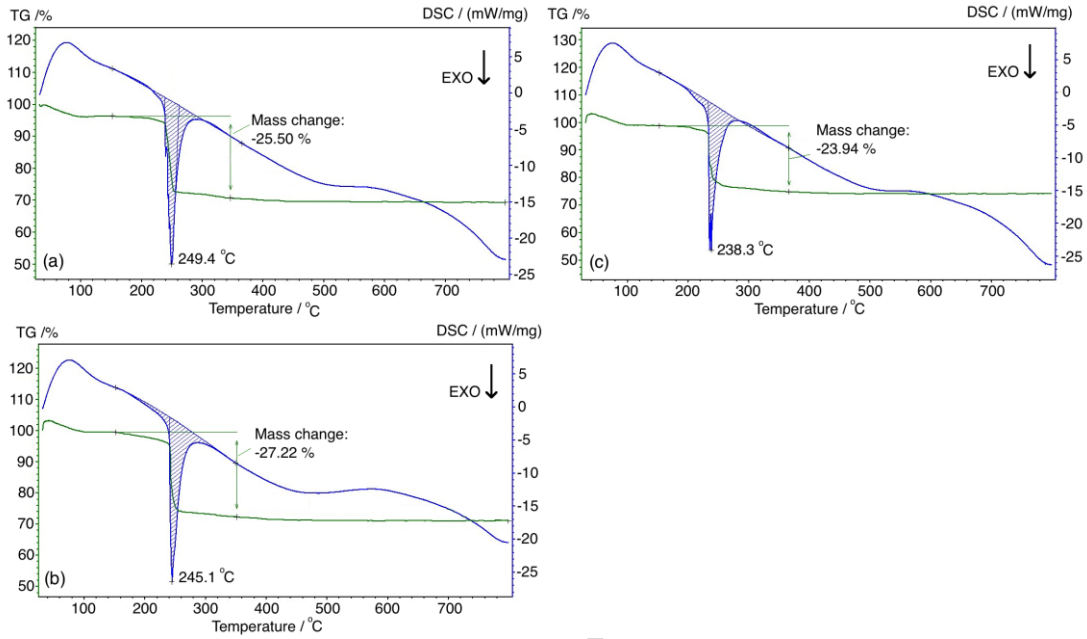

Fig. 3 TGA/DSC curves of Co-HLC-90 (a), Co-HLC-120 (b), and Co-HLC-150 (c).

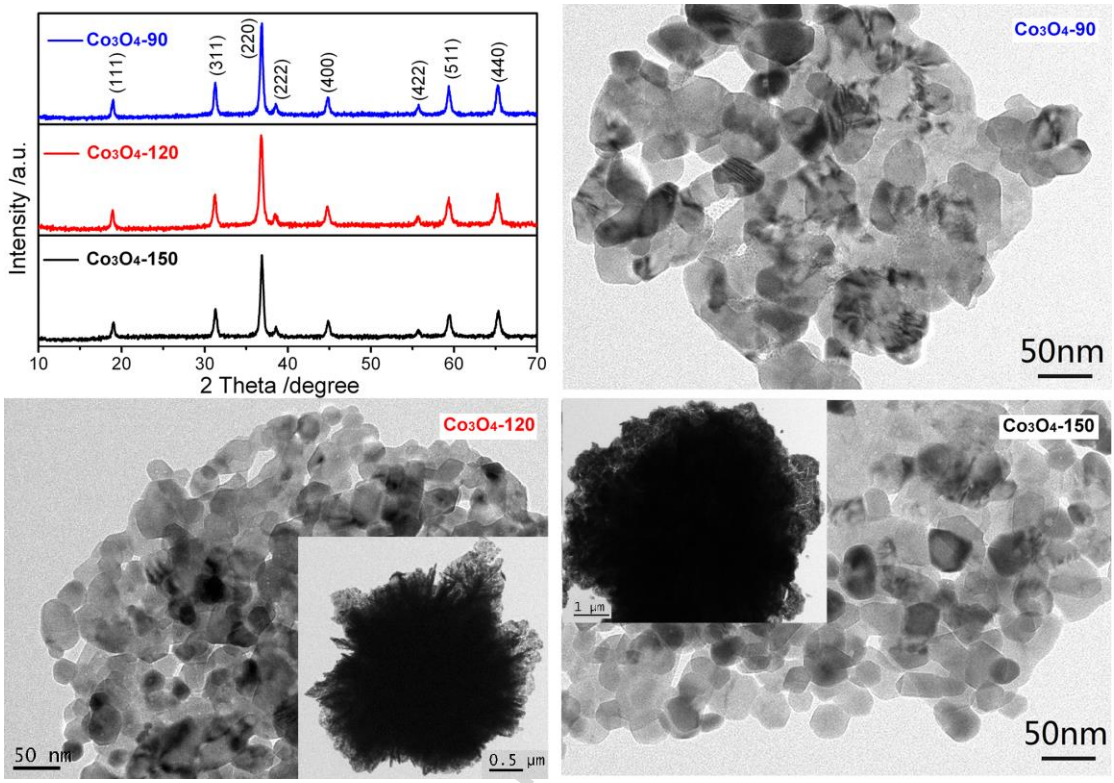

Fig. 4 XRD patterns and TEM images of Co_3O_4-90, Co_3O_4-120, and Co_3O_4-150, respectively.

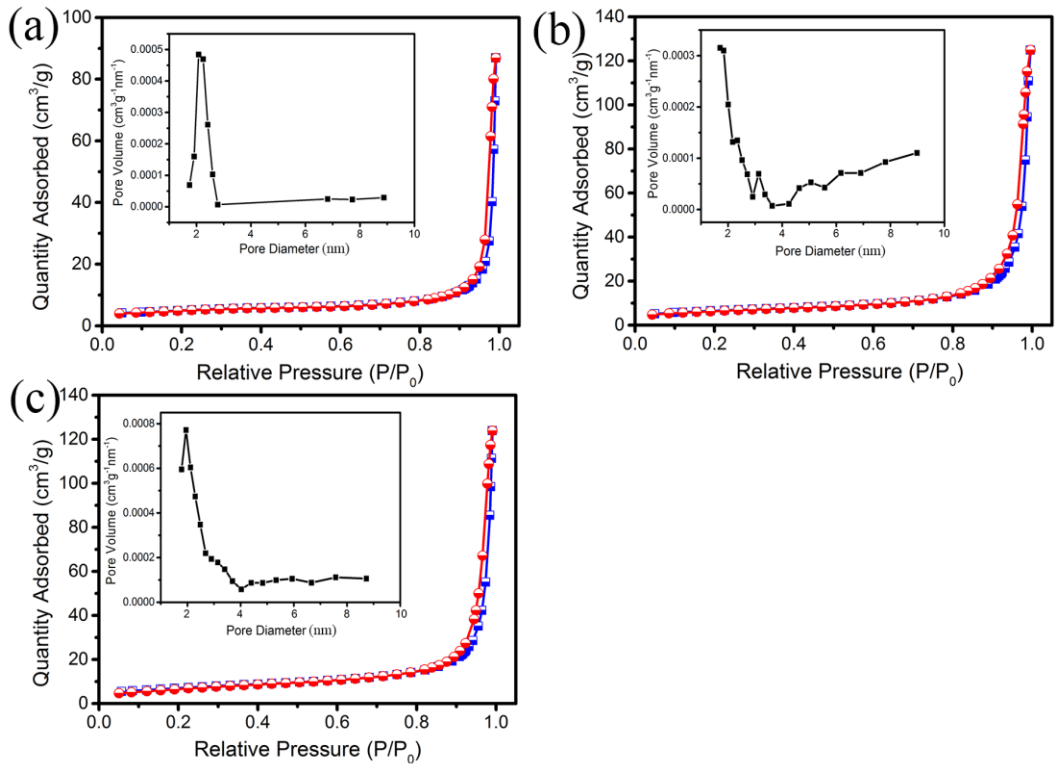

Fig. 5 N_2 adsorption−desorption isotherm of (a) Co_3O_4-90, (b) Co_3O_4-120, and (c) Co_3O_4-150. The inset in each isotherm is the corresponding pore size distributions.

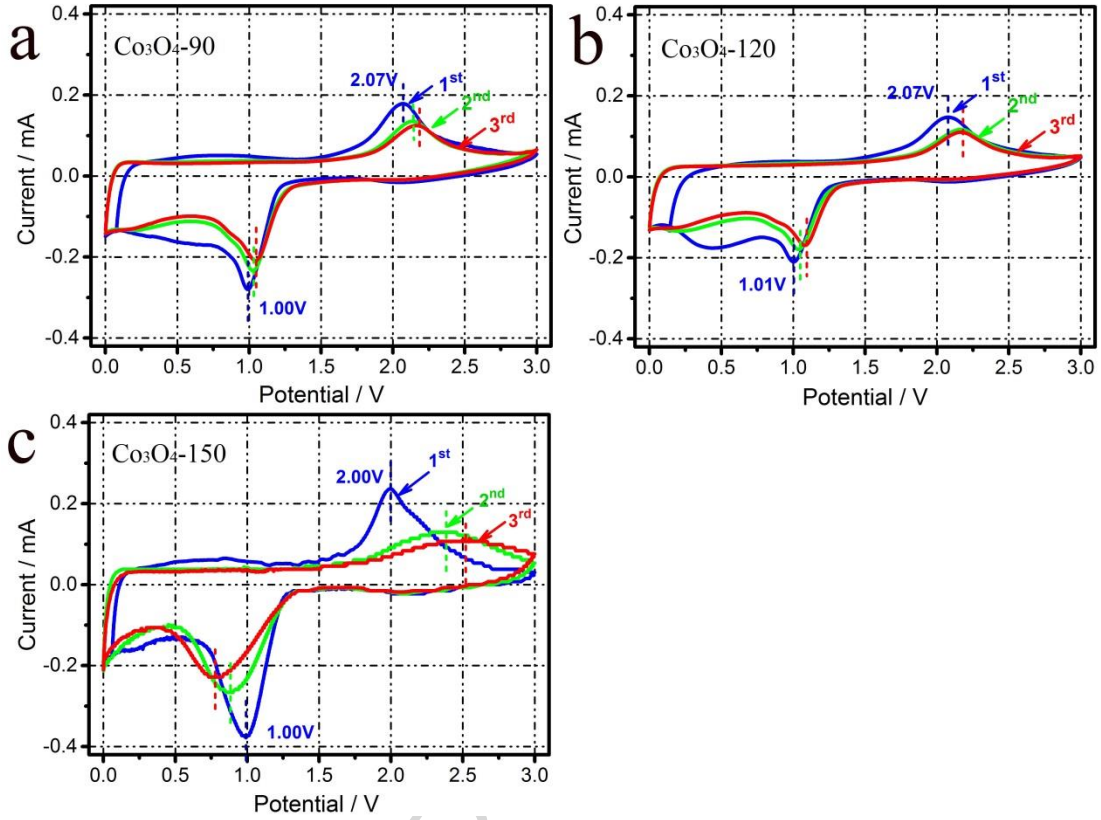

Fig. 6 The first three CV curves of (a) Co_3O_4-90, (b) Co_3O_4-120 and (c) Co_3O_4-150 at a scan rate 0.1 mV s^{-1}.

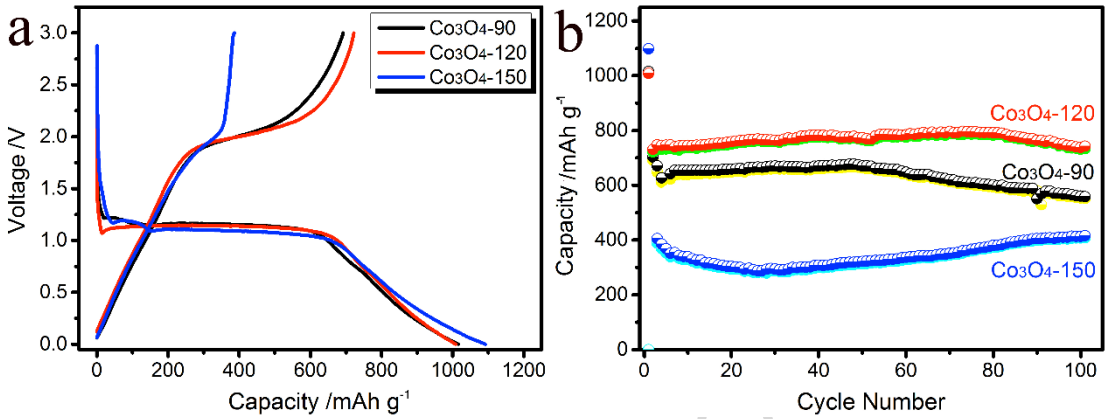

Fig. 7 The first charge-discharge cycles (a) and cycle performance (b) of the Co_3O_4 at the current density of 100 mA g^{-1}.

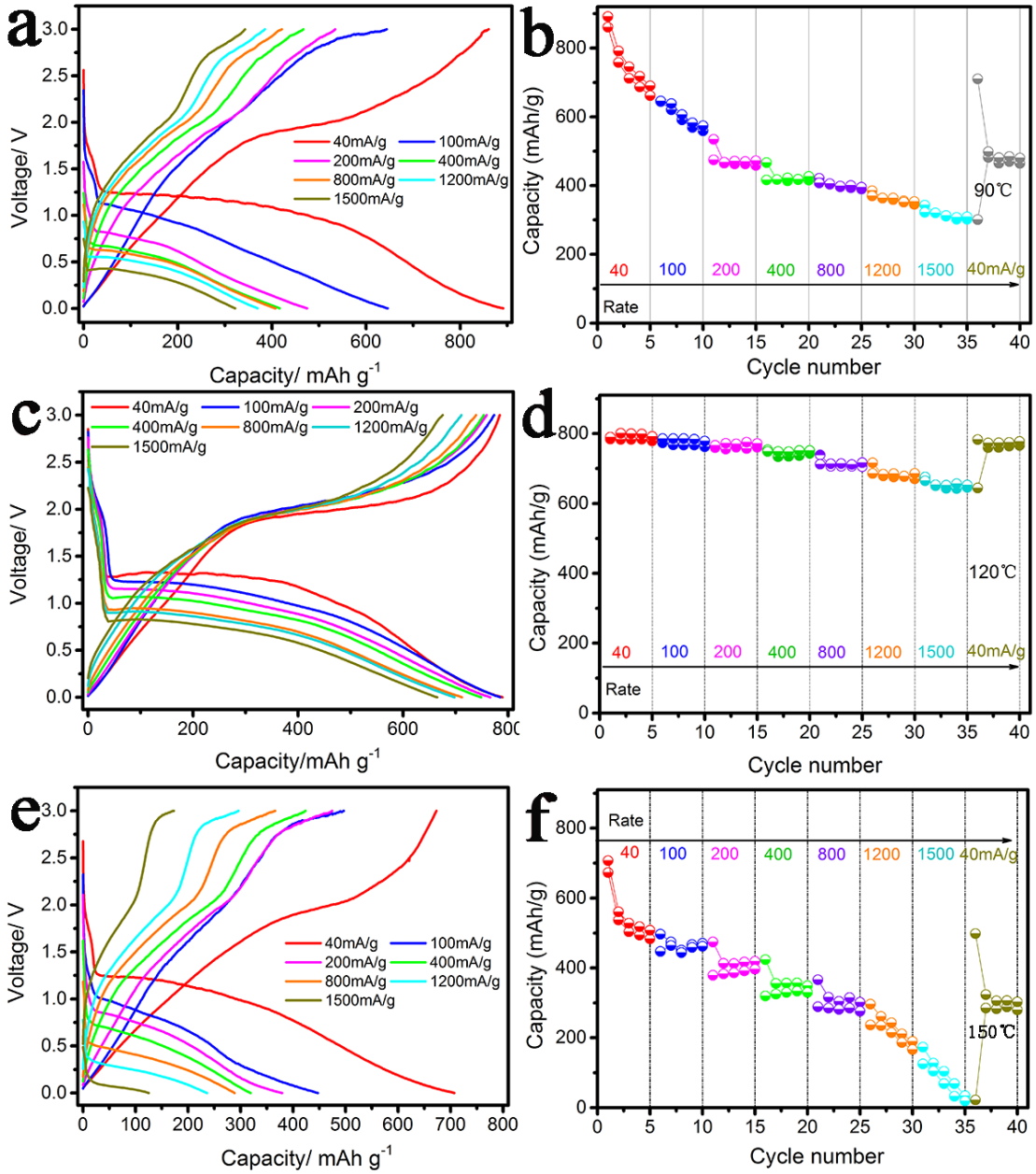

Fig. 8 The initial charge/discharge curves and rate performance of Co_3O_4-90 (a) and (b), Co_3O_4-120 (c) and (d), Co_3O_4-150 (e) and (f) carried out at various current densities.

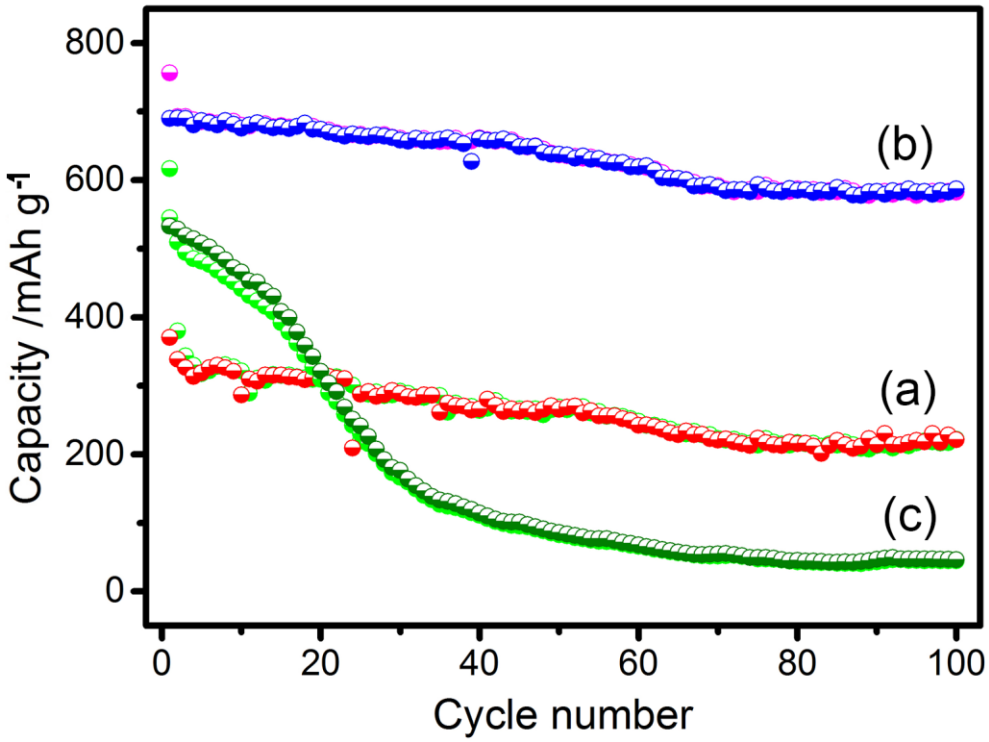

Fig. 9 The cyclic performance of Co_3O_4-90 (a), Co_3O_4-120 (b), Co_3O_4-150 (c) as anode worked at the current density of 800 mA g^{-1}.

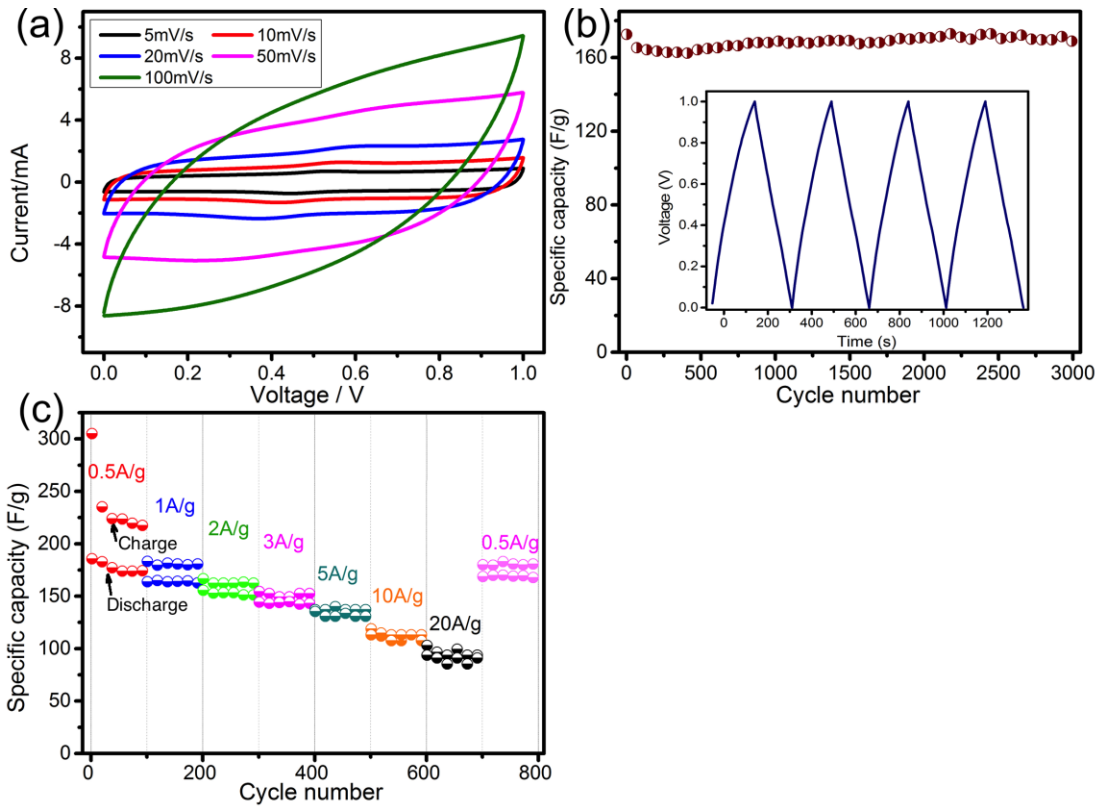

Fig. 10 The electrochemical performance of Co_3O_4-120 as electrode in a supercapacitor. The CV curves of Co_3O_4-120 electrode v.s. Hg/Hg_2Cl_2 carried out under various scanning rates (a). Cyclic supercapacitance and galvanostatic charge-discharge curves at 1 A g^{-1} (b). Rate performance of Co_3O_4-120 electrode at different current densities from 0.5 A g^{-1} to 20 A g^{-1}.

Graphic Abstract

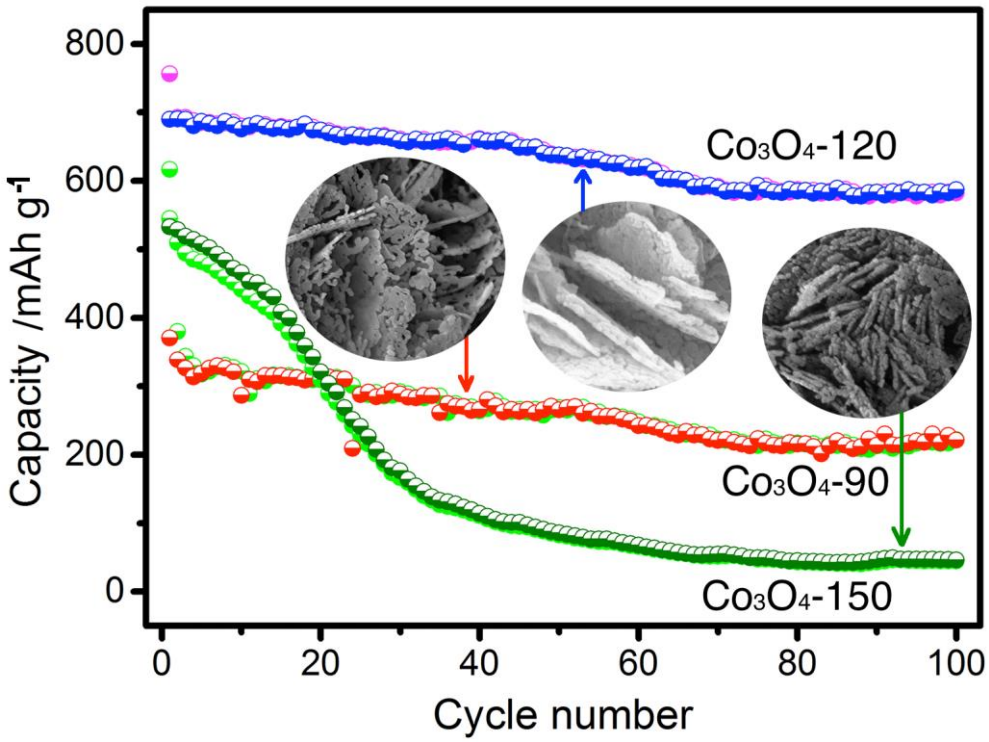

Highlight

Self-assembly cobalt hydrotalcite-like compounds were synthesized by refluxing.

Refluxing temperature plays the important role in particles morphology.

Co_3O_4 powders successfully maintained the architecture of the precursor after pyrolysis.

At 800 mA g^{-1}, Co_3O_4 releases 756 mAh g^{-1} and remains 582 mAh g^{-1} at the 100th cycle.